

New Olivine Reference Materials for In Situ Oxygen Isotope Determination

Juan Li,^{a,b} Shui-Jiong Wang,^{a,c} * Li-Guang Wu,^{a,b} Feng-Kun Li,^d and Xian-Hua Li^e

^aState Key Laboratory of Geological Processes and Mineral Resources, China University of Geosciences (Beijing), Beijing 100083, P. R. China

^bInstitute of Earth Sciences, China University of Geosciences (Beijing), Beijing 100083, P. R. China

^cFrontiers Science Center for Deep-time Digital Earth, China University of Geosciences (Beijing), Beijing 100083, P. R. China

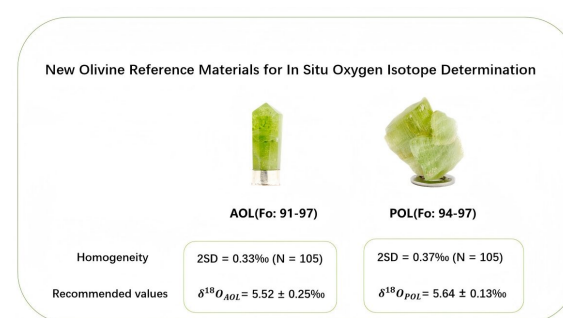
^dSchool of Earth Sciences and Resources, China University of Geosciences, Beijing 100083, P. R. China

^eInstitute of Geology and Geophysics, Chinese Academy of Sciences, Beijing 100029, P. R. China

Received: January 03, 2026; Revised: April 27, 2026; Accepted: May 09, 2026; Available online: May 09, 2026.

DOI: 10.46770/AS.2026.0001

ABSTRACT: Olivine is a key mineral of mafic-ultramafic and metamorphic rocks. Oxygen isotopic composition of olivine has been widely used to decipher mantle processes, igneous differentiation, and fluid-rock interaction in metamorphic systems. Accurate in situ oxygen isotopic analysis of olivine by secondary ion mass spectrometry (SIMS) requires matrix-matched reference materials to correct instrumental mass fractionation and monitor the stability of instrument. In this study, we report two natural olivine reference materials, AOL (Fo: 91-97) and POL (Fo: 94-97), for in situ oxygen isotopic analysis. These samples exhibit homogeneous oxygen isotopic compositions, with a two-standard deviation of 0.33‰ (N = 105) and 0.37‰ (N = 105), respectively. The recommended $\delta^{18}\text{O}$ values, determined by laser fluorination isotope ratio mass spectrometry, are $5.52 \pm 0.25\text{‰}$ for AOL and $5.64 \pm 0.13\text{‰}$ for POL (all $\pm 2\text{SD}$, N = 5). Combined with previously reported olivine standards, our results confirm that no significant matrix effects were observed within the forsterite (Fo) content range of Fo₉₁ to Fo₉₇, supporting the wide use of AOL and POL as reference materials for high-precision oxygen isotope microanalysis.



INTRODUCTION

Olivine is one of the most common rock-forming minerals in samples derived from the terrestrial mantle, asteroids, and comets.^{1, 2} Its oxygen isotopic ratios provide key insights into mass-dependent and mass-independent fractionation processes associated with rocks and mineral formation³⁻⁷. At mantle temperatures, oxygen isotopic fractionation between olivine and basaltic melt is generally $\leq 1\text{‰}$, and fractionation between olivine and coexisting minerals (e.g., orthopyroxene and spinel) is typically less than 1.5‰.⁸ These small fractionations highlight the importance of high precision measurements in resolving subtle isotopic variations.

Secondary ion mass spectrometry (SIMS) is a powerful technique for in situ oxygen isotopic analysis, offering permil-level precision and micrometer-scale spatial resolution.⁹ However,

the measured oxygen isotopic ratios by SIMS deviate from true values due to instrumental mass fractionation (IMF). This bias arises from a combination of SIMS analytical conditions and matrix effects of the target samples.¹⁰⁻¹² Thus, accurate determination of oxygen isotopes in olivine requires matrix-matched reference materials (RMs) with homogeneous chemical compositions and identical instrument conditions.¹³⁻¹⁶

Significant efforts have been made to develop suitable RMs and correct matrix effects in SIMS oxygen isotope analysis of olivine.^{4, 17-19} It is well established that the SIMS instrumental bias in olivine varies with chemical composition.^{20, 21} Recently, Isa *et al.*¹² established a calibration curve between Fe molar fractions (Fa = Fe / (Mg + Mn + Fe) mol%) and IMF using nine olivine reference materials spanning the full forsterite-fayalite series. Their results revealed that IMF in iron-rich olivine (Fa > 25) exhibits a stronger dependence on Fa content than in magnesium-rich olivine (Fa <

25),¹² providing a quantitative framework for correcting matrix effects in intermediate-composition olivines. Similar IMF variations among magnesium-rich olivines were confirmed by Scicchitano *et al.* and Tang *et al.*^{5,18} Zhang *et al.*⁴ developed seven new iron-rich olivine RMs and examined instrumental bias in a suite of olivine ($Fo = Mg / (Fe + Mg)$ mol%, $Fo = 0-100$), confirming its systematic correlation with Fo content.

Several other well-characterized natural olivines have been employed as reference materials. The widely used San Carlos olivine standard was developed by Gene Jarosewich and co-workers at the Smithsonian Institution.^{19,22} Peng *et al.* reported JAY03-3 and JAY03-4 as potential reference materials, with forsterite contents of 99.3% and 99.6%, respectively, but their homogeneity is limited, with SIMS oxygen isotopic measurement precision of 0.57‰ (2SD) for JAY03-3 and 0.70‰ (2SD) for JAY03-4.¹⁷ Although these natural standards have been critical in advancing in situ microanalysis, a shortage of well-characterized, homogeneous, and publicly available natural olivine RMs continues to hinder the progress in high-precision oxygen isotope research.

This study provides a rigorous evaluation of two potential natural olivine reference materials (AOL and POL). Each sample was analyzed at 105 individual spots for oxygen isotopes, demonstrating excellent internal uniformity ($2SD \leq 0.37\%$). Precise oxygen isotopic compositions were determined by laser fluorination isotope ratio mass spectrometry (LF-IRMS) method. These well-characterized, homogeneous samples are intended as publicly available reference materials, offering the community a reliable and accessible resource for high-precision in situ oxygen isotope microanalysis.

EXPERIMENTAL

Samples. This study focuses on two natural olivine samples: AOL (5.6 g from the Arizona district, USA) and POL (10.6 g, from Pakistan). All these crystals exhibit green coloration, as shown in Fig. 1(a-b). Each crystal was crushed into fragments of approximately 0.3 mm. Grains were manually selected for purity under a binocular microscope. In detail, 79 grains from AOL and 89 grains from POL were randomly selected and mounted in epoxy resin together with San Carlos olivine as a reference material. To minimize potential “X – Y effects” during SIMS analysis, all grains were positioned within 6 mm from the center of the mount.^{9,23} Subsequently, the mount was polished to obtain flat analytical surfaces and was coated with high-purity gold film (~30 nm). Inspection using high-magnification optical microscopy confirmed the transparency of the prepared grains. Additionally, a separate batch of crushed material from each sample was sieved to ~80 mesh for LF-IRMS oxygen isotope analysis.

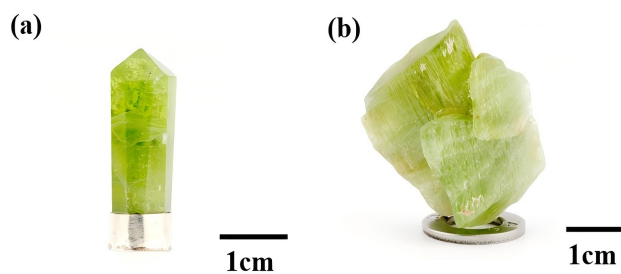


Fig. 1 Images of the AOL (a) and POL (b).

Imaging and electron microprobe analysis. Backscattered electron (BSE) imaging of the olivine grains was performed using a ZEISS field emission scanning electron microscope at the State Key Laboratory of Biogeology and Environmental Geology, China University of Geosciences, Beijing (CUGB). EPMA analysis was conducted using a JXA-8230 instrument at the Electron Probe Laboratory of the Institute of Mineral Resources, Chinese Academy of Geological Sciences. Measurements were conducted under the following operating condition: 15 kV accelerating voltage, 20 nA beam current, and a focused beam diameter of 5 μ m. A set of 12 elements (Si, Al, Mg, Fe, Cr, Mn, Na, K, Ca, Ni, Ti, and P) was analyzed and standardized using natural minerals and synthetic materials. Matrix corrections were applied using the ZAF correction procedure.

SIMS oxygen isotopic analysis. Oxygen isotopic measurements were conducted using CAMECA IMS 1300-HR3 at CUGB. A detailed analytical procedure has been reported in Li *et al.*²⁴ In brief, a primary ion beam of Cs^+ was accelerated to 10 kV with an intensity of ~3 nA. To minimize aberrations, the beam was operated in Gaussian mode rastered across a $5 \times 5 \mu m^2$ area. The spot size was ~15 μ m in diameter. Sample charging was compensated using a normal-incidence electron flood gun. Secondary ions of negative polarity were collected by applying an extraction potential of -10 kV. A field aperture of $5 \times 5 mm^2$ was used and the entrance slit was set to ~120 μ m. An energy window of 50 eV width was used. Magnetic field stability, maintained using a nuclear magnetic resonance probe, was better than 3 ppm over 16 hours. The signals of ^{16}O and ^{18}O were simultaneously collected on two Faraday cups (L2' and H2'), using amplifiers with 1010 Ω and 1011 Ω resistance, respectively. The slit #1 (500 μ m) on the multi-collector was used to achieve a mass resolution of ~2500 (50% peak width). The ^{16}O intensity ranged from 2.18×10^9 cps (counts per second) to 2.38×10^9 cps. Each spot analysis involved pre-sputtering, beam centering, and signal collection, with a total analytical time per spot of ~4 min, including 3.5 min for pre-sputtering and centering of the secondary beam, and 0.5 min for collection of 15 cycles of ^{16}O and ^{18}O signals. One to two spots were randomly selected on each grain to minimize sampling bias and enhance the representativity of the dataset. Reference materials

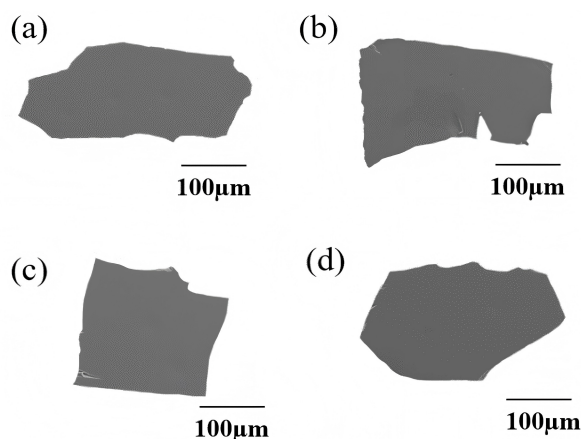


Fig. 2 Representative BSE images of AOL (a-b) and POL (c-d).

were analyzed after every 7-8 unknown samples to monitor the stability of the instrument. The measured $^{18}\text{O}/^{16}\text{O}$ ratios were normalized relative to the Vienna Standard Mean Ocean Water (VSMOW) composition ($^{18}\text{O}/^{16}\text{O} = 0.0020052$; Eq. 1).²⁵

$$(\delta^{18}\text{O})_{M(\text{raw})} = \left(\frac{(^{18}\text{O}/^{16}\text{O})_M}{0.0020052} - 1 \right) \times 1000\text{‰} \quad (1)$$

LF-IRMS oxygen isotopic analysis. LF-IRMS oxygen isotopic measurements were performed at the Institute of Geology and Geophysics (Beijing), Chinese Academy of Sciences (IGGCAS). A New Wave Research MIR10-30 laser was coupled to a vacuum extraction system.¹⁵ Samples with weights of ~ 1.5 mg were reacted with purified BrF_5 reagent in the sample chamber to liberate oxygen. The gases generated in the laser chamber were purified through a series of cryogenic traps held at liquid nitrogen temperature. The O_2 gas was analyzed using an MAT 252 mass spectrometer. The Penglai zircon ($\delta^{18}\text{O} = 5.31 \pm 0.10\text{‰}$)²⁶ and 04BXL07 garnet ($\delta^{18}\text{O} = 3.70 \pm 0.10\text{‰}$)²⁷ were analyzed together to monitor the stability of the instrument, which yielded a 2SD of $\pm 0.16\text{‰}$ and $\pm 0.22\text{‰}$, respectively.

RESULTS AND DISCUSSION

Microscopic features and chemical compositions. A total of ten BSE images of fragments from all olivine samples confirm textural homogeneity. No obvious chemical zoning was observed. During SIMS analysis, areas containing inclusions and cracks (Fig. 2) should be carefully avoided based on imaging.

The major element compositions of the olivine samples are summarized in Table 1 (with detailed data in Table S1). Based on twenty individual EPMA spot analyses, both samples are mainly composed of SiO_2 (about 41 wt%), MgO (about 53 wt%), and FeO (about 5 wt%), with minor NiO (about 0.23 wt%), Cr_2O_3 (about 0.01 wt%) and negligible Al_2O_3 . The Fo contents of the two olivine samples were 91-97 for AOL and 94-97 for POL.

SIMS oxygen isotopic data. SIMS oxygen isotope analyses of the two olivines were conducted in a single session to test their homogeneity and evaluate the matrix effects. A total of 105 spots were measured for each sample.

Throughout the analytical session, the San Carlos olivine standard yielded an external reproducibility of 0.29‰ (2SD, $N = 48$). This value is consistent with those reported by Qu *et al.*²³, confirming the analytical stability of the instrument. Natural olivines exhibit a wide range of $\delta^{18}\text{O}$ values, from 3.3 to 7.2‰, as documented in previous studies.^{3, 6, 28} Therefore, all obtained homogeneity values fall within the acceptable precision range for igneous rock analysis. The complete dataset is provided in Table S2.

The two olivine samples yield homogeneous oxygen isotopic compositions, with overall variations (2SD) of 0.33‰ for AOL and 0.37‰ for POL. The data for each sample follow a Gaussian distribution (Fig. 3), and the standard error (1SE) of individual analyses is within 0.1‰. No significant linear correlation is observed between the measured $\delta^{18}\text{O}$ values and the X-coordinates of the analytical spots for any of the samples (Fig. 4). The $\delta^{18}\text{O}$ values cluster around their mean values, indicating that the “X–Y effects” are small and negligible compared to the analytical uncertainty.

LF-IRMS oxygen isotopic data. All precise oxygen isotope data were obtained by IRMS. Based on five replicate analyses per sample, the mean $\delta^{18}\text{O}_{\text{IRMS}}$ values with two standard deviations are $5.52 \pm 0.25\text{‰}$ for AOL and $5.64 \pm 0.13\text{‰}$ for POL. All LF-IRMS oxygen isotopic data are listed in Table S3.

Matrix effect. This study evaluates potential matrix effects in SIMS oxygen isotope analysis of olivine with notable variations in Fo content. To quantify the matrix effect, instrumental mass fractionation (IMF) was calculated using the following equation:

$$\text{IMF} = \delta^{18}\text{O}_{\text{SIMS}_N} - \delta^{18}\text{O}_{\text{IRMS}} \quad (2)$$

Table 1. The major and minor chemical composition (wt. %) of the olivine samples.

Sample	Na_2O	SiO_2	Al_2O_3	K_2O	CaO	NiO	MnO	FeO	MgO	TiO_2	Cr_2O_3	P_2O_5	Total	Fo, mean(range) (mol %)
AOL	0.01	41.23	0.00	0.00	0.00	0.25	0.04	5.51	52.33	0.01	0.01	0.00	99.42	94(91-97)
POL	0.00	41.42	0.00	0.00	0.00	0.23	0.04	4.40	53.29	0.01	0.01	0.01	99.42	96(94-97)

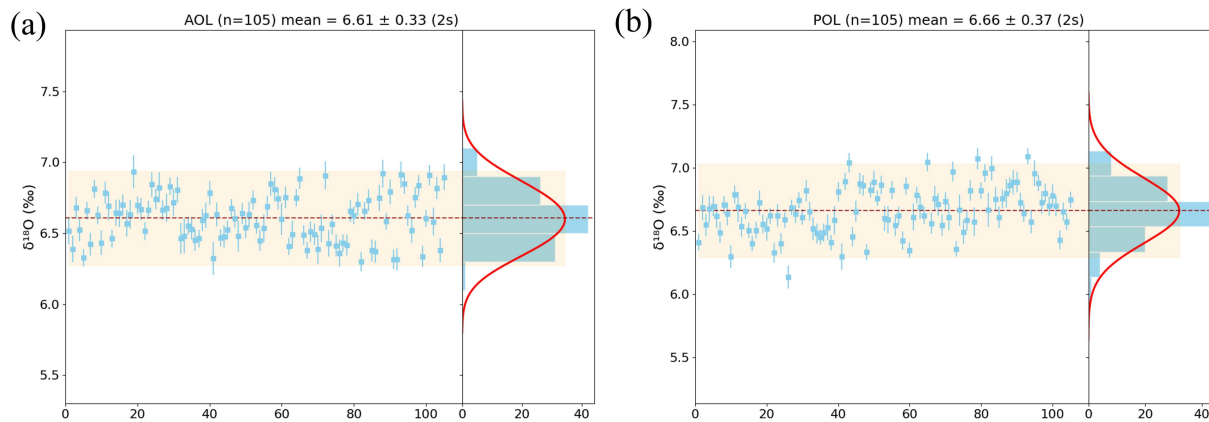


Fig. 3 Histogram of $\delta^{18}\text{O}$ measured values for AOL and POL determined by SIMS.

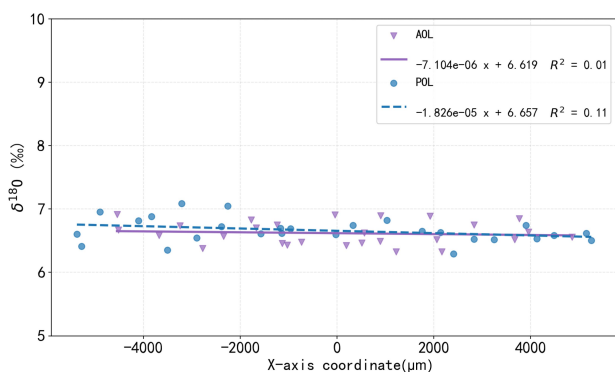


Fig. 4 Correlation diagram of measured $\delta^{18}\text{O}$ values by SIMS vs. X-axis coordinate for AOL and POL.

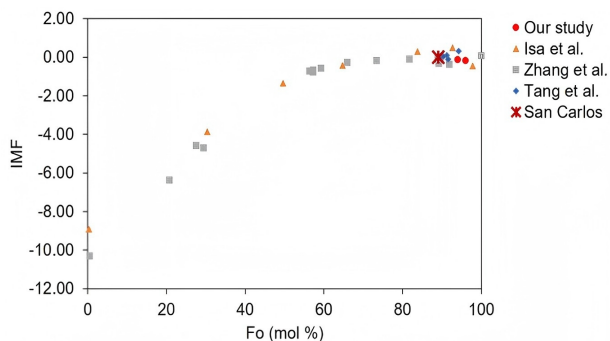


Fig. 5 IMF values of olivine samples vs. Fo (mol%). * San Carlos IRMS and Fo data are from Kita *et al.*²¹.

where $\delta^{18}\text{O}_{\text{SIMS}_N}$ represents the raw value that has been referenced to San Carlos ($\delta^{18}\text{O} = 5.32\text{‰}$) measured in a SIMS session and $\delta^{18}\text{O}_{\text{IRMS}}$ is the recommended value from LF-IRMS. The uncertainty of IMF (2s) is estimated as:

$$2S_{\text{IMF}} = \sqrt{\left(\frac{2S_{\text{SIMS}}}{\sqrt{N_{\text{SIMS}}}}\right)^2 + \left(\frac{2S_{\text{IRMS}}}{\sqrt{N_{\text{IRMS}}}}\right)^2} \quad (3)$$

where $2S_{\text{SIMS}}$ and $2S_{\text{IRMS}}$ denote the two-standard-deviation variabilities of SIMS and IRMS analyses, respectively, while N_{SIMS} and N_{IRMS} represent the corresponding number of replicate measurements.

As listed in Table 2, IMF values for the studied olivines (Fo = 91–97) fall within a limited range (-0.19‰ to -0.12‰). This variation is negligible relative to the analytical precision of the method ($\sim 0.37\text{‰}$, 2SD for SIMS; $\sim 0.25\text{‰}$, 2SD for IRMS), indicating that matrix effects are minimal across this Fo interval. This conclusion is further corroborated by the homogeneous oxygen isotopic compositions of AOL (Fo = 91–97) and POL (Fo = 94–97), which remain within analytical uncertainty even within samples that exhibit a wide range of Fo values.

Our results are consistent with previous studies on magnesium-rich olivines (Fig. 5). Isa *et al.*¹² noted minimal IMF variation in olivines with Fo > 75, while Zhang *et al.* noted that the values of bias are nearly invariant among magnesian olivine (Fo > 60).⁴ Tang *et al.* observed no significant matrix effects across Fo = 89.6–94.2.¹⁸ This consistency confirms that these well-characterized olivines within the Fo 91–97 range are suitable as matrix-matched RMs for high-precision *in situ* oxygen isotope analysis.

CONCLUSION

In this study, the oxygen isotopic homogeneity of two olivine samples was characterized, and recommended values of oxygen isotope composition for these samples were determined with the LF-IRMS method. Both olivines exhibit homogeneous oxygen isotopic compositions, with overall variations (2SD) less than 0.37‰, and no significant matrix effect was found within the Fo range of 91–97.

Together with recently developed olivine standards, AOL and

Table 2. SIMS oxygen isotope data for olivine samples with varying Fo values, including two standard deviations (2SD) and number of replicates (N). The last column presents the IMF and its associated 2SD (2sIMF), calculated using Eq. (2) and Eq. (3), respectively

Condition	sample	Fo (mol %)	$\delta^{18}\text{O}_{\text{SIMS}_N}$ (‰)	$\delta^{18}\text{O}_{\text{IRMS}_N}$ (‰)	IMF (‰)
This study IMS-1300	AOL	94.00	5.40 ± 0.33 (N = 105)	5.52 ± 0.25 (N = 5)	-0.12 ± 0.12
	POL	96.00	5.45 ± 0.37 (N = 105)	5.64 ± 0.13 (N = 5)	-0.19 ± 0.07
	San Carlos	89.00	5.32 ± 0.29 (N = 48)	5.32 ± 0.08 (N = 3)	0.00 ± 0.09
Isa et al.¹² IMS-1290	Pine river	97.80	4.02 ± 0.60 (N = 3)	4.48	-0.46
	Mt. Franklin	92.60	5.42 ± 0.20 (N = 5)	4.92	0.50
	Urals	83.80	6.62 ± 0.20 (N = 5)	6.33	0.29
	Skaergaard EG 5108	64.70	4.12 ± 0.20 (N = 5)	4.54	-0.42
	NWA6693	49.60	2.52 ± 0.40 (N = 6)	3.86	-1.34
	Skaergaard EG 1907	30.30	0.42 ± 0.20 (N = 6)	4.28	-3.86
	Rock Port	0.30	-4.18 ± 0.60 (N = 12)	4.74	-8.92
Zhang et al.⁴ IMS-1280	HN-OI	100.00	8.96 ± 0.07 (N = 4)	8.90 ± 0.08 (N = 3)	0.06 ± 0.06
	HaK-OI	91.90	4.86 ± 0.19 (N = 21)	5.25 ± 0.04 (N = 3)	-0.39 ± 0.06
	IG-OI	89.60	5.13 ± 0.20 (N = 10)	5.23 ± 0.03 (N = 3)	-0.10 ± 0.07
	UW-OI-1	89.20	5.16 ± 0.14 (N = 10)	5.48 ± 0.11 (N = 5)	-0.32 ± 0.07
	SW-OI	81.80	3.41 ± 0.18 (N = 21)	3.51 ± 0.03 (N = 2)	-0.10 ± 0.04
	FJ-OI	73.40	4.72 ± 0.37 (N = 22)	4.89 ± 0.28 (N = 3)	-0.17 ± 0.18
	SK90-5-OI	66.00	4.32 ± 0.28 (N = 18)	4.61 ± 0.16 (N = 3)	-0.29 ± 0.11
	OR-OI	59.30	5.31 ± 0.21 (N = 4)	5.88 ± 0.02 (N = 3)	-0.57 ± 0.11
	SK90-8-OI	57.30	3.91 ± 0.35 (N = 19)	4.60 ± 0.11 (N = 3)	-0.69 ± 0.10
	SK90-6-OI	57.30	3.89 ± 0.47 (N = 19)	4.67 ± 0.20 (N = 3)	-0.78 ± 0.16
	SK90-9-OI	56.40	3.89 ± 0.29 (N = 20)	4.63 ± 0.40 (N = 3)	-0.74 ± 0.24
	SK90-22-OI	29.40	-0.16 ± 0.33 (N = 19)	4.55 ± 0.14 (N = 3)	-4.71 ± 0.11
	SK90-21-OI	27.60	-0.07 ± 1.32 (N = 19)	4.52 ± 0.48 (N = 2)	-4.59 ± 0.45
	SK90-14-OI	20.80	-1.94 ± 0.34 (N = 20)	4.45 ± 0.09 (N = 3)	-6.39 ± 0.09
Fa50278-OI	0.54	-5.81 ± 0.34 (N = 7)	4.50	-10.31	
Tang et al.¹⁸ IMS-1280	06JY06OL	89.60	5.20 ± 0.18 (N = 25)	5.20 ± 0.06 (N = 3)	0.00 ± 0.05
	06JY29OL	91.20	5.40 ± 0.30 (N = 40)	5.30 ± 0.26 (N = 4)	0.10 ± 0.14
	06JY31OL	90.30	5.32 ± 0.34 (N = 40)	5.27 ± 0.30 (N = 4)	0.05 ± 0.16
	06JY34OL	91.50	5.15 ± 0.28 (N = 39)	5.25 ± 0.14 (N = 2)	-0.10 ± 0.11
	09XDTC1-24OL	94.20	4.22 ± 0.20 (N = 40)	3.91 ± 0.50 (N = 3)	0.31 ± 0.29

POL provide a valuable addition to the current suite of RMs. These well-characterized samples offer researchers a more diverse and reliable set of tools for high-precision oxygen isotope analysis, facilitating further investigations into a wide range of geological and geochemical processes. These olivines are available for public use as oxygen isotope RMs for in situ microanalysis.

ASSOCIATED CONTENT

The data supporting this article (Tables S1-S3) is available at <https://www.at-spectrosc.com>

AUTHOR INFORMATION



Shui-Jiong Wang received his BSc in 2008 and PhD in 2013 from the China University of Geosciences (Beijing). He is a professor of geochemistry at China University of Geosciences (Beijing). His major research interests are metal stable isotope geochemistry and isotopic microanalysis, and their applications to igneous petrogenesis, chemical geodynamics and evolution of Earth and Moon. Shui-Jiong Wang is author or co-author of over 50 articles published in peer-reviewed scientific journals.

Corresponding Author

* S.-J. Wang

Email address: wsj@cugb.edu.cn

Notes

The authors declare no competing financial interest.

ACKNOWLEDGMENTS

This study was supported by the National Natural Science Foundation of China (42521005) and the Fundamental Research Funds for the Central Universities (2652023001).

REFERENCES

1. J. C. M. De Hoog, L. Gall, and D. H. Cornell, *Chem. Geol.*, 2010, **270**, 196-215. <https://doi.org/10.1016/j.chemgeo.2009.11.017>
2. N. Nekrylov, P. Y. Plechov, Y. D. Gritsenko, M. V. Portnyagin, V. D. Shcherbakov, V. A. Aydov, and D. Garbe-Schönberg, *Am. Mineral.*, 2021, **106**, 206-215. <https://doi.org/10.2138/am-2020-7566>
3. H. Yu, H.-F. Zhang, H. Zou, and J.-F. Xu, *Am. Mineral.*, 2022, **107**, 904-913. <https://doi.org/10.2138/am-2022-7990>
4. M. Zhang, K. Fukuda, M. J. Spicuzza, G. Siron, A. Heimann, A. J. Hammerstrom, N. T. Kita, T. Ushikubo, and J. W. Valley, *Chem. Geol.*, 2022, **608**, 121016. <https://doi.org/10.1016/j.chemgeo.2022.121016>
5. M. R. Scicchitano, D. Rubatto, J. Hermann, A. S. Majumdar, and A. Putnis, *Chem. Geol.*, 2018, **499**, 126-137. <https://doi.org/10.1016/j.chemgeo.2018.09.020>
6. J.-Y. Xu, A. Giuliani, Q.-L. Li, K. Lu, J. C. Melgarejo, and W. L. Griffin, *Nat. Commun.*, 2021, **12**, 6295. <https://doi.org/10.1038/s41467-021-26668-z>
7. D. Ouyang, H. Bao, G. R. Byerly, and Q. Li, *Commun. Earth Environ.*, 2024, **5**, 34. <https://doi.org/10.1038/s43247-023-01197-3>
8. J. M. Eiler, *Rev. Mineral. Geochem.*, 2001, **43**, 319-364. <https://doi.org/10.2138/gsrmg.43.1.319>
9. N. T. Kita, T. Ushikubo, B. Fu, and J. W. Valley, *Chem. Geol.*, 2009, **264**, 43-57. <https://doi.org/10.1016/j.chemgeo.2009.02.012>
10. J. M. Eiler, C. Graham, and J. W. Valley, *Chem. Geol.*, 1997, **138**, 221-244. [https://doi.org/10.1016/S0009-2541\(97\)00015-6](https://doi.org/10.1016/S0009-2541(97)00015-6)
11. J. M. Huberty, N. T. Kita, R. Kozdon, P. R. Heck, J. H. Fournelle, M. J. Spicuzza, H. Xu, and J. W. Valley, *Chem. Geol.*, 2010, **276**, 269-283. <https://doi.org/10.1016/j.chemgeo.2010.06.012>
12. J. Isa, I. E. Kohl, M. C. Liu, J. T. Wasson, E. D. Young, and K. D. McKeegan, *Chem. Geol.*, 2017, **458**, 14-21. <https://doi.org/10.1016/j.chemgeo.2017.03.020>
13. A. Wudarska, M. Wiedenbeck, E. Slaby, M. Lempart-Drozd, C. Harris, M. M. Joachimski, C. Lécuyer, K. G. MacLeod, A. Pack, T. Vennemann, F. Couffignal, D. Feng, J. Clodny, C. Kusebauch, S. Mayanna, X. Rocholl, L. Speir, Y. Sun, and F. D. H. Wike, *Geostand. Geoanal. Res.*, 2022, **46**, 277-306. <https://doi.org/10.1111/ggr.12416>
14. G.-Q. Tang, Y. Liu, Q.-L. Li, L.-J. Feng, G.-J. Wei, W. Su, Y. Li, G.-H. Ren, and X.-H. Li, *Atom. Spectrosc.*, 2020, **41**, 188-193. <https://doi.org/10.46770/AS.2020.05.002>
15. L. Feng, H. Li, and T. Li, *Minerals*, 2020, **10**, 987. <https://doi.org/10.3390/min10110987>
16. Y. Li, G.-Q. Tang, Y. Liu, S. He, B. Chen, Q.-L. Li, and X.-H. Li, *Chem. Geol.*, 2021, **582**, 120445. <https://doi.org/10.1016/j.chemgeo.2021.120445>
17. B. Peng, M. He, M. Yang, and Y. Shi, *Crystals*, 2023, **13**, 987. <https://doi.org/10.3390/cryst13070987>
18. G.-Q. Tang, B.-X. Su, Q.-L. Li, X.-P. Xia, J.-J. Jing, L.-J. Feng, L. Martin, Q. Yang, and X.-H. Li, *Geostand. Geoanal. Res.*, 2019, **43**, 585-593. <https://doi.org/10.1111/ggr.12288>
19. K. Qu, H. Wu, and G.-Q. Tang, *Appl. Sci.*, 2025, **15**, 2445. <https://doi.org/10.3390/app15052445>
20. J. W. Valley and N. T. Kita, Secondary Ion Mass Spectrometry in the Earth Sciences, *Mineralogical Association of Canada*, 2009. <https://doi.org/10.3749/9780921294818>
21. N. T. Kita, H. Nagahara, S. Tachibana, S. Tomomura, M. J. Spicuzza, J. H. Fournelle, and J. W. Valley, *Geochim. Cosmochim. Acta*, 2010, **74**, 6610-6635. <https://doi.org/10.1016/j.gca.2010.08.011>
22. E. Jarosewich, J. A. Nelen, and J. A. Norberg, *Geostand. Newsl.*, 1980, **4**, 43-47. <https://doi.org/10.1111/j.1751-908X.1980.tb00273.x>
23. P. Peres, N. T. Kita, J. W. Valley, F. Fernandes, and M. Schuhmacher, *Surf. Interface Anal.*, 2013, **45**, 553-556. <https://doi.org/10.1002/sia.5061>
24. J. Li, S.-J. Wang, L.-G. Wu, X.-H. Li, J.-H. Hao, and J.-J. Xu, *J. Anal. At. Spectrom.*, 2026, **41**, 702-707. <https://doi.org/10.1039/D5JA00344J>
25. Baertschi, *Earth Planet. Sci. Lett.*, 1976, **31**, 341-344. [https://doi.org/10.1016/0012-821X\(76\)90115-1](https://doi.org/10.1016/0012-821X(76)90115-1)
26. X. H. Li, W. G. Long, Q. L. Li, Y. Liu, Y. F. Zheng, Y. H. Yang, K. R. Chamberlain, D. F. Wan, C. H. Guo, X. C. Wang, and H. Tao, *Geostand. Geoanal. Res.*, 2010, **34**, 117-134. <https://doi.org/10.1111/j.1751-908X.2010.00036.x>
27. B. Gong, Y.-F. Zheng, and R.-X. Chen, *Phys. Chem. Miner.*, 2007, **34**, 687-698. <https://doi.org/10.1007/s00269-007-0184-4>
28. P.-P. Liu, D.-B. Wang, M.-F. Zhou, X.-H. Li, Q.-L. Li, G. A. Gaetani, B. Monteleone, and V. Kamenetsky, *Geology*, 2023, **52**, 161-165. <https://doi.org/10.1130/g51690.1>